JOURNAL OF MATERIALS SCIENCE 25 (1990) 3976–3981

Interstitial segregation and embrittlement in Ti–6Al–4V alloy

Y. B. XU
Laboratory of Fatigue and Fracture for Materials, Institute of Metal Research, Academia Sinica, Shengyang 110015, People's Republic of China
Z. S. XU
Northeast Institute of Technology, People's Republic of China

The investigation into the microstructural characteristics of the segregation found occasionally in Ti–6Al–4V alloy showed that the segregated region was enriched in titanium but impoverished in aluminium and vanadium. It was also found that the interstitial content of oxygen and nitrogen was higher in the segregated region. The effect of the segregation on the mechanical properties of the alloy was also studied. The tensile strength, ductility and toughness of specimens with segregation were reduced to compare with values for as-received specimen. The micro-fracture mechanism associated with this segregation was analysed. The results revealed that the plastic deformation is mainly of shear mode in slip band. Microcracks were nucleated preferentially within the segregated region and this is believed to be the cause of brittle fracture on the basal plane (0 0 0 1) and prismatic plane (1 0 $\bar{1}$ 0) in the hexagonal close packed lattice.

1. Introduction

Titanium alloys are widely used in weight-critical applications such as airframe and gas turbine engines, because of their specific strengths. The extensive service experience accumulated during the past few years has proved that great attention must be paid to controlling the metallurgical quality in the production and application of these alloys. One of the metallurgical quality problems is the local segregation associated with the interstitial impurities.

The reaction of the titanium alloy with oxygen is significant, leading to a loss of strength and ductility as well as toughness. As some authors have pointed out [1–3], the room-temperature ductility of α-titanium is significantly influenced by interstitial solute, and it is embrittled by as little as 1.2 at % dissolved oxygen.

This paper presents the results of an investigation into the structural characteristics of the local segregation in Ti–6Al–4V alloy and its influence on the mechanical properties as well as on the microfracture mechanism associated with this segregation.

TABLE I Chemical composition (wt %)

Al	V	Fe	Si	N	O	C	H	Ti
6.14	4.23	0.11	0.05	0.02	0.13	0.005	0.005	Balance

2. Materials and Procedure

The alloy used for the present study was melted in VAF and the ingots forged. The chemical composition of the as-received material is given in Table I.

The specimens cut from disc material were divided into two groups, with and without segregation, for the microstructural examinations and the mechanical tests. Tensile tests were conducted on a servohydraulic

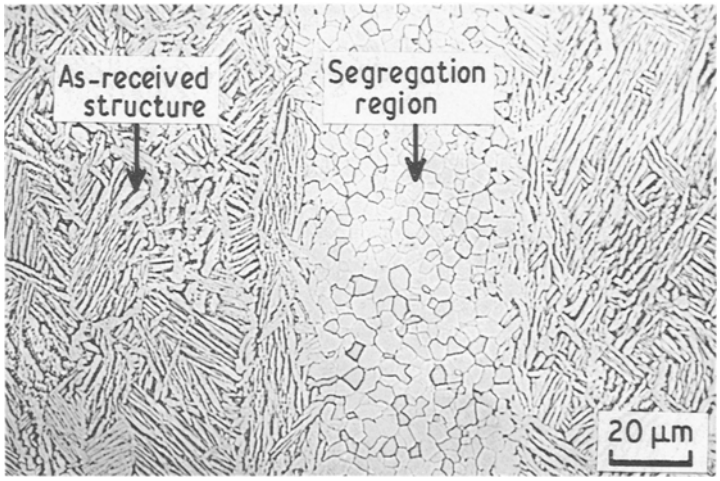

Figure 1 Microstructure consisting of both the segregation region (α-phase) and the as-received structure (α + β-phases).

0022–2461/90 $03.00 + .12

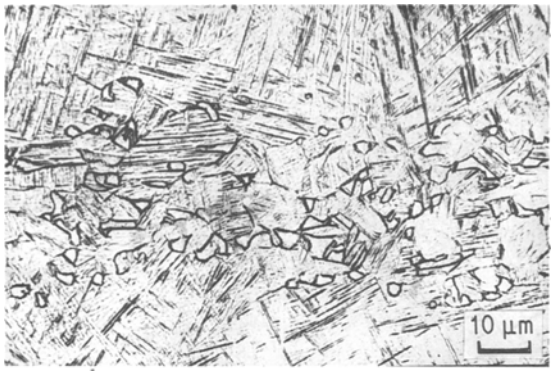

Figure 2 Microstructure at 1050° C for 1 h, water-quenched.

testing machine at room temperature. Fracture toughness measurement was determined by three-point bend test. The fracture surfaces of the tensile and fracture toughness test pieces were examined by scanning electron microscopy (SEM). Specimens for optical microscopy were mechanically polished and then chemically etched in a solution of 25% HNO_3 + 50% H_2O + 25% HF. Observations by transmission electron microscopy were performed on a Philips 420 electron microscope operated at 100 kV. The thin-foil specimens for transmission electron microscopy (TEM) were prepared using a twin-jet polishing apparatus and electrolyte consisting of a solution of 25% HNO_3 + 25% HF + 50% H_2O. Microanalysis for titanium, aluminium and vanadium, particularly for oxygen and nitrogen was conducted on a type MS46 electron probe microanalyser.

Among the various techniques used the most successful attempt was made to observe the dynamic process of microcrack nucleation and propagation during deformation by using a tensile stage fitted within an SEM.

3. Results

A typical microstructure characteristic of a specimen with segregation which was subjected to annealing at 800° C for 1 h and then air-cooled is illustrated in Fig. 1. It can be seen from this figure that there are two quite distinct regions in this condition. One is single α-phase and is referred to as the segregation or defect region, and the other is the as-received structure ($\alpha + \beta$ phases). The single α-phase appears with β + transformed β-phase and original β-phase grew quickly when the specimen was heated at 1050° C for 1 h as shown in Fig. 2. It seems that the transformation temperature for the segregation region is significantly higher.

A series of thin-foil observations by TEM show that the dislocation structure in the segregation region (Fig. 3) is quite different from that found in the as-received structure (Fig. 4) and the dislocation density in this region is considerably higher than that for the as-received structure. Electron diffraction analysis proved that the segregation region was mainly composed of α-phase with hexagonal packed structure, as shown in Fig. 5.

X-ray diffraction analysis was made of the segregation region (Fig. 6b) and the as-received structure

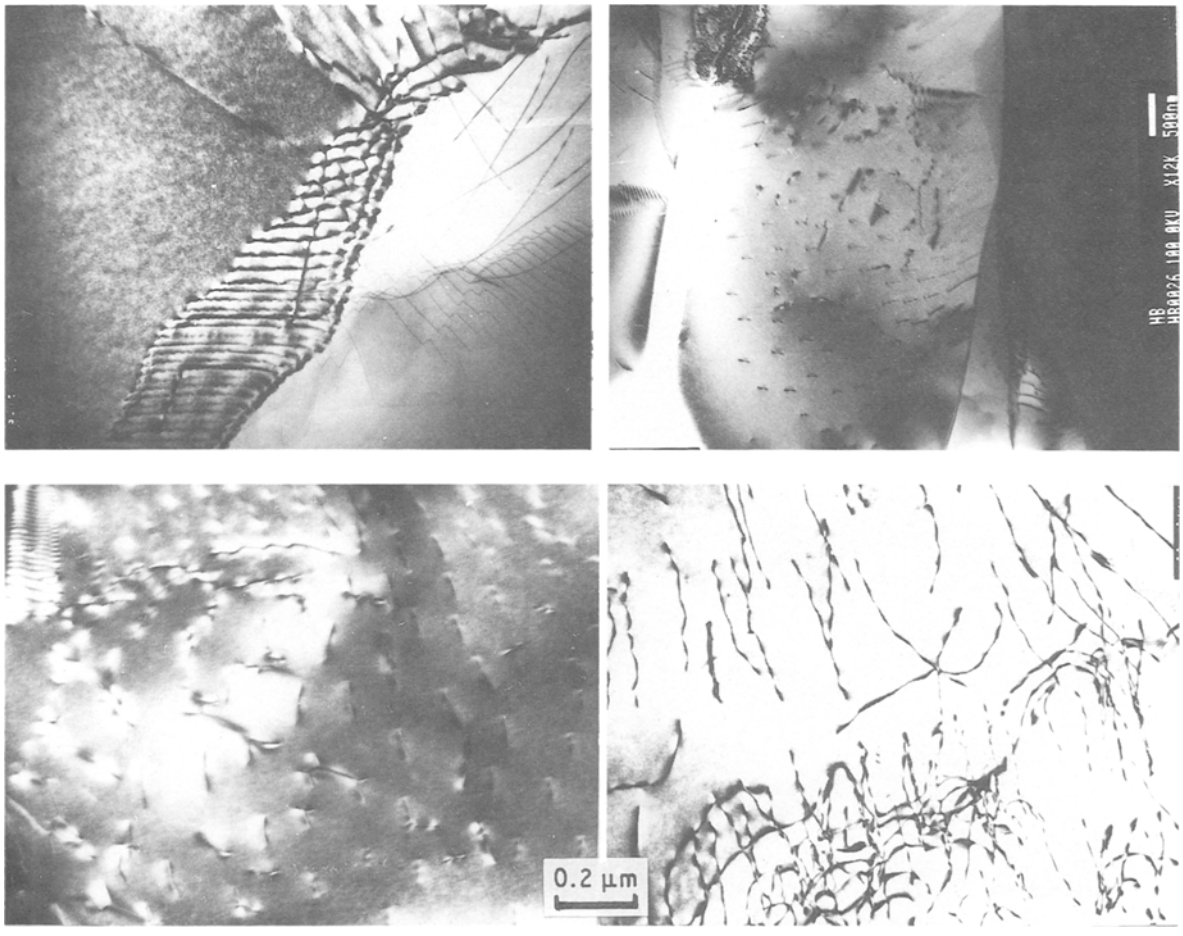

Figure 3 TEM thin-foil micrographs, showing dislocation substructure in the segregation region.

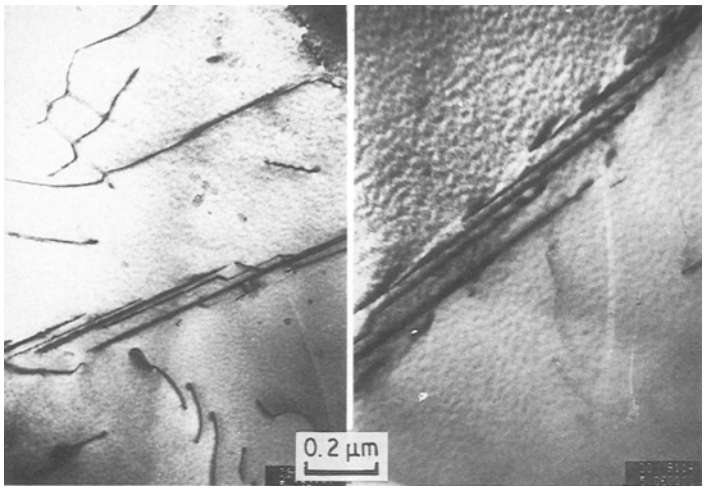

Figure 4 Dislocation substructure in the as-received structure.

(Fig. 6a) which were air-cooled after annealing at 800° C for 1 h. From comparison of these diffraction patterns, it is clear that a new strong peak just near the α-phase occurred in the segregation region besides α and β peaks arising from α- and β-phases, and it is referred to as α_L-phase.

To confirm further this new finding, the lattice constants were calculated from these patterns. The results show that they are $a = 0.2945$ nm and $c = 0.4703$ nm for α_L-phase, compared with the known value of $a = 0.2930$ nm and $c = 0.4672$ nm for α-phase. Note that the ratio $c/a = 1.597$ for α_L-phase is much larger than that for α-phase in HCP structure ($c/a = 1.549$). Therefore, it is reasonable to assume that the unit cell for α_L-phase in the segregation region is expanded by the interstitial impurities oxygen and nitrogen.

In order to compare the difference in alloying element and interstitial impurities between the segregation region and the as-received structure, microanalysis was made for titanium and aluminium, and particularly for oxygen and nitrogen. Many point-by-point data determined indicated that the average contents of oxygen and nitrogen in the segregation region are considerably higher than those of the as-received structure.

The segregation coefficient calculated is 5 for oxygen and 1.5 for nitrogen in the segregation region relative to the as-received structure. The average segregation coefficients for titanium, aluminium and vanadium are 1.1, 0.8 and 0.7, respectively, indicating that the segregation region is enriched in titanium but impoverished in aluminium and vanadium.

Two sets of specimens, one with and the other without the segregation, were chosen to evaluate its influence on the properties of the alloy.

Room-temperature tensile properties for both specimens are summarized in Table II. Fig. 7 shows their stress-strain curve. It can be clearly seen that the yield strength and ultimate tensile strength for the specimen with the segregation are considerably lower than those for the as-received specimen. The difference is probably due to the local segregation of impurities which is known to affect flow stress in titanium alloy.

The fracture toughness tests were conducted on the specimens (dimensions 10 mm × 10 mm × 55 mm) with and without segregation using a three-point bending method. A fatigue precrack was introduced by a testing machine with high frequency, so that the plastic zone of the crack was made just to touch the edge of the segregation region as shown schematically in Fig. 8.

It was found that the specimen with segregation exhibited a distinct load drop at maximum load and sometimes a load plateau eared on the load displacement curve, whereas the as-received specimen exhibited a slight amount of crack-tip plasticity before maximum load was reached.

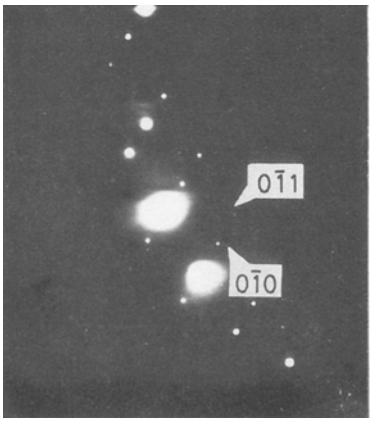

Figure 5 Electron diffraction pattern of the segregation region with zone axis [$\bar{1}$ 0 0].

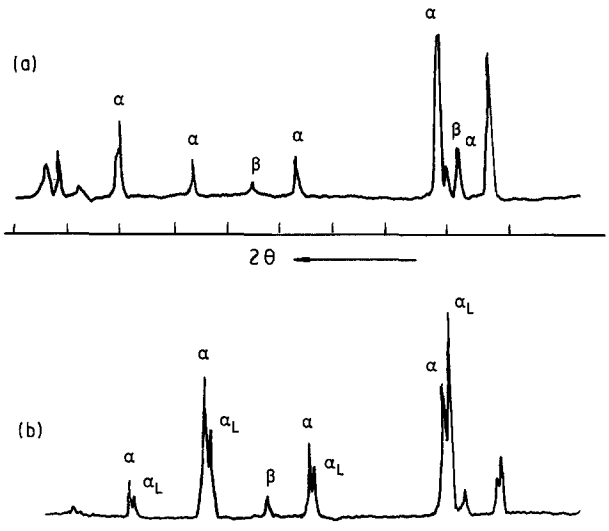

Figure 6 X-ray diffraction patterns from both the as-received structure and the segregation regions.

TABLE II Tensile properties

Specimens	Yield strength (MPa)	UTS (MPa)	Elongation (%)	Reduction in area (%)
As-received	854.46	956.48	11.8	35.6
With segregation	795.27	918.26	8.6	30.2

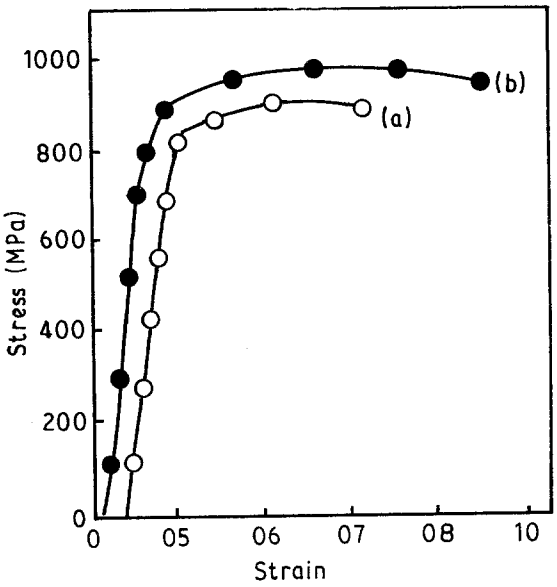

Figure 7 Stress-strain curve for both specimens with and without the segregation.

According to the expressions

$$K_Q = \frac{P_Q Y(a/w)}{BW^{1/2}} \quad \text{and} \quad K_{max} = \frac{P_{max} Y(a/w)}{BW^{1/2}}$$

where P_{max} is the maximum load, P_Q is the load as determined in the *Annual Book of Standards* [4], B is the specimen thickness, W is the specimen depth and a is the crack length, K_Q and K_{max} were calculated and the results are summarized in Table III.

It is obvious that the segregation of impurities lowered the fracture toughness and the resistance to crack propagation significantly compared with those of the specimens free from the segregation. They are reduced by 34 and 33% respectively.

The fracture surface morphology was observed by SEM. The specimen that was free from segregation had a ductile-fibrous fracture as is evidenced by the typical shear dimples shown in Fig. 9. The fracture surface of the segregation region was rather smooth and flat at low magnification, but at high magnification in the SEM the fracture exhibited two types of morphology, resembling quasi-cleavage fracture in steel. As shown in Fig. 10, one type, which was very often observed, looks like a lotus-leaf (Fig. 10a). The other looks like a willow-leaf (Fig. 10b).

The etch-pit technique was used to study the mechanism of fracture which is caused by the segregation.

TABLE III Summary of the fracture toughness results

Specimens	K_Q(MPa m$^{1/2}$)	K_{max}(MPa m$^{1/2}$)
With segregation	51.43	50.45
As-received	63.66	63.0

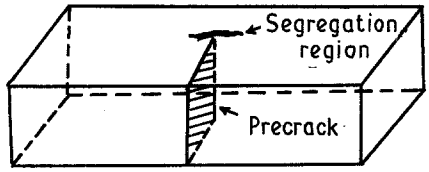

Figure 8 Schematic diagram showing the segregation region position in the fracture toughness specimen.

The fracture surface was etched by an aqueous solution of 25 ml HNO_3 + 5 ml HF + 8 ml H_2O for 20 sec and then immediately examined in the SEM. It was observed that the lotus-leaf-like surface exhibited hexagonal pits in the shape shown in Fig. 11a, whereas the willow-leaf-like fracture exhibited rectangular ones as shown in Fig. 11b. From etch-pit analysis, it is suggested that the former, the lotus-leaf-like fracture, is caused by cleavage on the basal plane (0 0 0 1) and the latter, willow-leaf-like, is caused by cleavage on the prismatic plane (1 0 $\bar{1}$ 0). In other words, the fracture for the segregation region is as a result of the cleavage on the (0 0 0 1) or (1 0 $\bar{1}$ 0) planes in the HCP structure.

The microdeformation and fracture of specimens with and without segregation was examined *in situ* by SEM. Crack nucleation was located and the path of crack propagation was followed during loading. It was found that cracks initiated preferentially in the segregation region but not in the as-received structure when the specimen was subjected to tensile load as shown in Fig. 12. Plastic deformation in the segregation region is mainly of shear mode on the slip band making an angle of 45° with the tensile axis, as shown in Fig. 13. It was interesting to note that slip bands were interrupted at the grain boundary but no crack formed at the end of the bands. However, cracking along the bands occurred during deformation. Such a phenomenon was also found by Lai [5] in Ti–7Al–4Mo

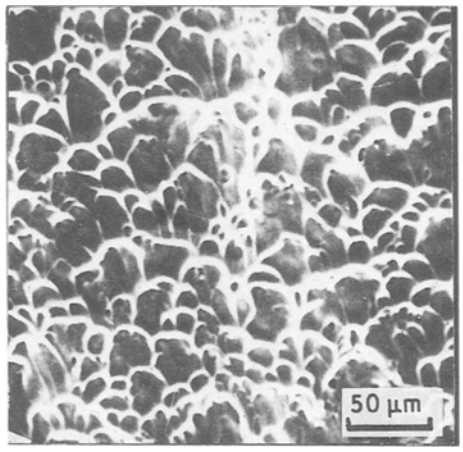

Figure 9 Topography of the fracture surface of the as-received specimen.

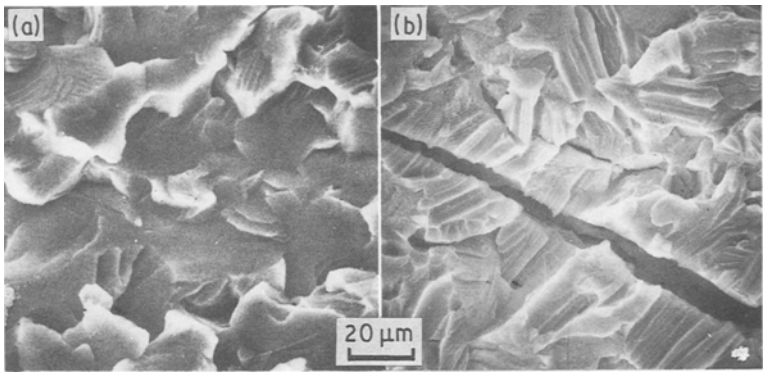

Figure 10 Microtopographs of (a) the lotus-leaf-like and (b) the willow-leaf-like fracture surface.

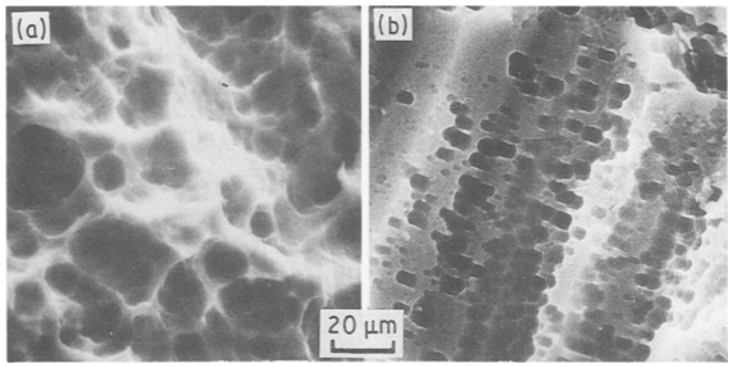

Figure 11 Etching pits on two kinds of fracture surface in the segregation region.

alloy and by one of the authors in high-carbon steel [6]. It is obvious that the shear stress along the bands is responsible for crack nucleation, and the magnitude of the stress for nucleation depends on the length of slip band [7]. A crack, once nucleated, will propagate along the band under the action of shear and normal stresses at the crack-tip [8]. From Fig. 14, it can also be seen that the shear crack is much more even and straight, characteristic of brittle fracture, unlike that found in the as-received structure. Fig. 15 shows the nucleation and propagation of a crack in the as-received structure during deformation. It is characteristic of ductile fracture, as evidenced by the deformation modes on both sides of the crack propagation path.

Based on the above results, it is clear that the segregation region in this alloy is much more brittle and is probably a source for brittle fracture under tensile load.

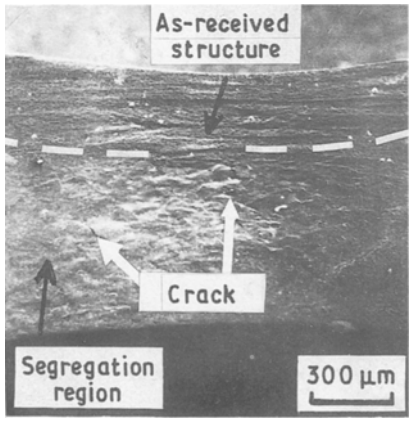

Figure 12 Initiation of microcracks in the segregation region during deformation (tensile axis is horizontal).

4. Discussion and Conclusions

Defects associated with the segregation of alloying elements and impurities have been reported elsewhere. Vicki [9] found four kinds of defects in Ti–6Al–4V alloy. One occurs as voids surrounded by interstitial-stabilized α-phase. The segregation region in which no voids and inclusions were found in the present study is little different from those found in Vicki's work.

It is well known that oxygen and nitrogen are strong α-stabilizing elements which interact with titanium. There are two types of interstitial sites in the HCP lattice and there will be three sets of slip systems: the prismatic plane $(1\,0\,\bar{1}\,0)$, the pyramidal plane $(1\,0\,\bar{1}\,1)$ and basal plane $(0\,0\,0\,1)$ with a common slip direction $\langle 1\,1\,\bar{2}\,0\rangle$. It is obvious that the segregation of interstitial impurities oxygen and nitrogen increases the resistance to dislocation motion as well as the critical resolved stress for slip on the $(1\,0\,\bar{1}\,0)$, $(1\,0\,\bar{1}\,1)$ and $(0\,0\,0\,1)$ planes [10, 11]. Gupta and Weinig [2] have studied the dislocation-oxygen interaction in α-titanium

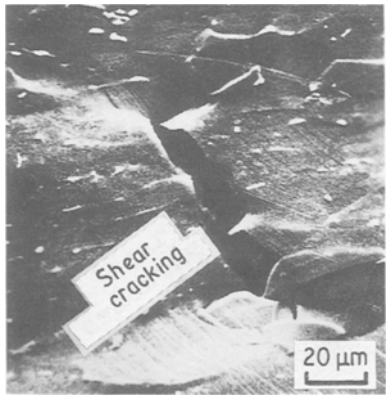

Figure 13 Shear deformation bands in the segregation region.

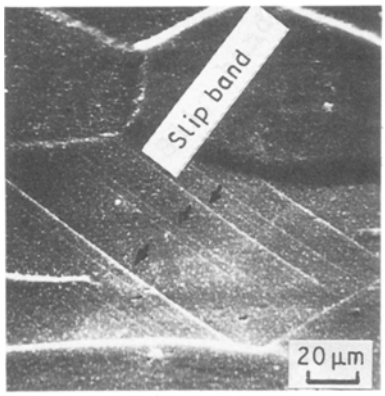

Figure 14 Cracking along the shear bands.

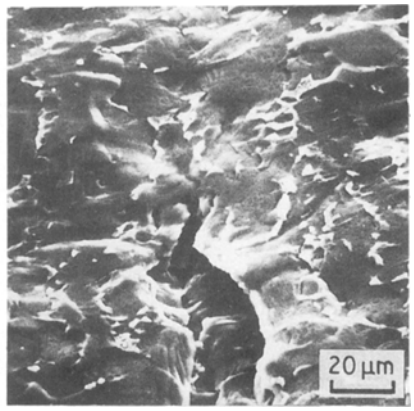

Figure 15 Microcrack propagation in the as-received structure.

and its effect on the ductile-to-brittle transition. They have pointed out that the brittle behaviour is a function of the solute atom-dislocation interaction. It was found in the present study that the dislocation structure in the segregation region is distinctly different from that of the as-received structure, and that the dislocation density is considerably higher. It is suggested that the intense interaction between the dislocation and the interstitial impurities occurred in the segregation region. Therefore, it is believed that the loss of both strength and toughness is considered to be due to the incorporation of oxygen and nitrogen atoms into the metal lattice, which is in agreement with the results of Shamblem and Radden [1]. In other words the dislocation pinning by impurities oxygen and nitrogen is responsible for the embrittlement of the segregation region in this alloy.

Fracture surface observations and etch-pit analysis show that fracture of the segregation region consists of two types of morphology: one lotus-leaf-like, and the other willow-leaf-like. Their cleavage planes are $(0\,0\,0\,1)$ and $(1\,0\,\bar{1}\,0)$, respectively.

The results from dynamic tensile tests show that deformation takes place mainly on the shear band and that nucleation of microcracks is initiated preferentially in the segregation region. Brittle fracture is as a result of shear cracking along maximum shear stress in two slip systems $(0\,0\,0\,1)\langle 1\,1\,\bar{2}\,0\rangle$ and $(1\,0\,\bar{1}\,0)\langle 1\,1\,\bar{2}\,0\rangle$.

References

1. C. E. SHAMBLEN and T. K. RADDEN, *Titanium Sci. Technol.* (1968) 199.
2. D. GUPTA and S. WEINIG, *Trans. AIME* **215** (1959) 209.
3. K. E. WIEDEMANN, R. N. SHENOY and J. UNNAM, *Trans. Metall.* **18A** (1987) 1503.
4. Annual Book of Standards, p. 519.
5. Z. H. LAI, in Proceedings of the Fourth International Conference on Titanium, 1980, Vol. 3, p. 1757.
6. Y. B. XU, *J. Scanning Electron Microsc.* **1** (1986) 43.
7. Y. B. XU, *Trans. Metall.* **18A** (1987) 1923.
8. D. A. KOSS and K. S. CHAN, *Acta Metall.* **28** (1980) 1245.
9. F. J. VICKI, *Titanium Sci. Technol.* **1** (1973) 167.
10. A. T. CHURCHMAN, *Proc. R. Soc.* **226A** (1954) 214.
11. P. G. PARTRIDGE, *Metal Mater. Met. Rev.* **11** (1967) 167.

Received 28 November 1988
and accepted 8 May 1989